Chapter 12
Photoluminescence Micro-imaging Sheds New Light on the Development of Metal Soaps in Oil Paintings

Mathieu Thoury, Annelies Van Loon, Katrien Keune, Joen J. Hermans, Matthieu Réfrégiers, and Barbara H. Berrie

Abstract This paper describes a photoluminescence imaging approach coupled to a synchrotron source (SR-PL imaging) that provides a new, powerful way to probe the processes involved in metal soap formation in paint films, processes that play an important role in the deterioration of paint films in traditional and modern oil paintings.

The technique couples multispectral PL mapping with sub-micrometer spatial resolution with the ability to tune the excitation radiation from UV-C to the visible range. False-color RGB images of the distribution of PL from three historical paint cross sections (two with lead soaps and one with zinc soaps) using a range of

M. Thoury (✉)
IPANEMA, CNRS, ministère de la Culture et de la Communication, Université de Versailles Saint-Quentin-en-Yvelines, Muséum National d'Histoire Naturelle, USR 3461, Université Paris-Saclay, Gif-sur-Yvette, France
e-mail: mathieu.thoury@synchrotron-soleil.fr

A. Van Loon
Conservation Department, Rijksmuseum, Amsterdam, The Netherlands

K. Keune
Conservation Department, Rijksmuseum, Van't Hoff Institute for Molecular Sciences, University of Amsterdam, Amsterdam, The Netherlands

J. J. Hermans
Van't Hoff Institute for Molecular Sciences, University of Amsterdam, Amsterdam, The Netherlands

M. Réfrégiers
Synchrotron SOLEIL, Gif-sur-Yvette, France

B. H. Berrie
National Gallery of Art, Washington, DC, USA

F. Casadio et al. (eds.), *Metal Soaps in Art*, Cultural Heritage Science,
https://doi.org/10.1007/978-3-319-90617-1_12

excitation and emission wavelengths were obtained. The resulting maps of PL from lead soaps within the cross sections provide new insight about their formation, which can be visualized occurring around lead white particles or flocs of particles as an initial step. Inhomogeneity within an individual lead soap aggregate is revealed and it can be seen that the aggregated forms have complex structures. A single aggregate in one sample was found to comprise five phases.

High spatial resolution images of the distribution of zinc soaps throughout a ZnO-containing paint film show that the periphery of small fissures containing soaps show luminescence of zinc oxide particles and no sign of a gradient in PL into the paint film, and thus allow inferring that Zn soap formation is not initiated at cracks, but rather soaps accumulate in them. Haloes of high luminescence around particles of emerald green implicate it in the development of Zn soaps.

These results show the potential of SR-PL imaging to provide improved characterization of Pb and Zn soap structures, leading to a better understanding of the kinetics of their formation and the development of macroscopic aggregates.

Keywords Lead soaps · Zinc soaps · Oil paintings · Degradation · Lead white · Zinc white · Photoluminescence · Synchrotron · Microscopy

12.1 Introduction

Many steps in the development of soaps in paintings remain incompletely understood, including the initiation factors, the rate of formation of soaps, and alteration and aggregation of the initial products. These are being studied using spectroscopic and chromatographic methods, but photoluminescence (PL) has not been used to a large extent, despite the observation that under UV-A irradiation aggregated lead and zinc soaps in paint films exhibit heterogeneous luminescence (Higgitt et al. 2003; Noble et al. 2002).

With the aim of performing an in-depth study of the luminescence properties of metal soaps and to establish the value of PL for investigating soap formation in oil paint films, at even very early stages, a novel synchrotron luminescence deep-UV imaging approach has been optimized and used to study the phenomenon. Developments in synchrotron deep-UV photoluminescence (SR-DUV-PL), micro-imaging implemented at the DISCO beam-line of synchrotron SOLEIL in collaboration with IPANEMA, have allowed the collection of unprecedented, detailed PL data on lead and zinc soaps at the submicron scale. The results rely on several factors in the set-up. Multi-spectral detection, optimized to collect emission from 300 to 1000 nm, in combination with a fully tunable deep-UV excitation wavelength allows unique spatial and spectral contrast between phases aggregated within metal carboxylate species that form as alteration products in oil paints. The full-field detection of luminescence makes it possible to obtain images of the distribution of PL in defined spectral ranges from large areas, even hundreds of square micrometers, with a spatial resolution of several hundred nanometers (Thoury et al. 2011). The high spatial dynamics attainable offers a new method for visualization and speciation

within diverse structures and morphologies of metal soap alteration products found in typical cross-section samples, providing a better understanding of their evolution over time, from the earliest stages up to formation of large aggregates of soaps that are apparent on the surfaces of paintings.

To illustrate the potential of the PL full-field micro-imaging set-up for studying soap formation, this paper presents examples of its application to two lead soap-containing and one zinc soap-containing paint samples that present different manifestations of and stages in the development of metal soaps in oil paint films. A cross-section sample taken from a large painting on canvas by Jacob Jordaens, *Revolt of the Batavian against Roman Rule* (1661–66, Royal Palace, Amsterdam), shows an early stage of lead soap formation, at which the lead white particles are in the process of converting into soaps, while a paint sample taken from a seventeenth-century ceiling painting depicting *Justitia and Mars in a Warm Embrace* (1680, Room of Trustees, Burgerweeshuis, Zierikzee) illustrates a mature stage with aggregation of lead soaps within the paint film. The sample taken from a painting by Vincent van Gogh, *Roses* (1890, National Gallery of Art, Washington), reveals the formation of zinc soaps throughout the paint layer. The interpretation of the PL data is supported by other analytical techniques, including scanning electron microscopy backscatter electron imaging (SEM-BSE) and attenuated total reflection Fourier-transform infrared (ATR-FTIR) micro-imaging.

12.2 Experimental

12.2.1 Samples and Sample Preparation

The samples were prepared at the different institutions following the in-house protocols. The sample of the Jordaens painting, sample N103 CS9, was embedded in a polyester resin (Polypol PS230, Poly-Service Amsterdam). The sample of the historic ceiling painting from the Burgerweeshuis in Zierikzee, sample ZZ7210_x12, was embedded in a methacrylate mounting resin (Technovit 2000 LC, Heraeus Kulzer GmbH, Germany). The sample from van Gogh's *Roses* was embedded in Bio-Plastic™ resin (Ward's Science). The samples were wet-ground on a polishing wheel to expose the complete paint layer build-up, with the assistance of a sample holder. In the final steps, Micro-Mesh® sheets up to grit 12,000 (Micro-Surface Finishing Products Inc., Wilton, Iowa, USA) were used for dry polishing (Van Loon et al. 2005). Each sample is described more fully in the Results section.

12.2.2 UV/VIS Spectral-imaging Setup at Disco

SR-DUV-PL experiments were performed using the full-field micro-imaging TELEMOS set-up of the DISCO beamline (Bertrand et al. 2013; Giuliani et al. 2009). The monochromatic synchrotron beam is coupled to a modified Zeiss Axio Observer

Z1 microscope (Carl Zeiss, Germany) equipped with a 100×/NA 1.25 immersion objective and a Princeton PIXIS 1024B/BUV EM-CCD (1024 × 1024 pixels, 13 μm pixel size), in front of which a filter wheel is positioned. This configuration allowed collection of images of the luminescence from the samples with spatial resolution to 150 nm. For examination of the PL from the Jordaens and the *Roses* samples, excitation wavelengths were set at 280 and 390 nm. For the Zierikzee sample, several excitation wavelengths were used: 240, 260, 280, 340, 360 and 380 nm. All emission images were acquired in nine spectral bands between 327 and 870 nm using high transmittance band-pass interference filters and with two dichroic mirrors with 300 and 400 nm cut-off wavelength, respectively. Visualization of the distribution of emission was improved by assigning images of interest to red (R), green (G) and blue (B) channels. The intensities of each channel of the full-field RGB image were either stretched between the 2nd and 98th percentile or linearly stretched using the ENVI 5.0 software (EXELIS) to facilitate visual comparison and discrimination of the distribution of the materials having different emission spectra.

12.2.3 Light Microscopy, Scanning Electron Microscopy and ATR-FTIR Imaging

Light microscopy of the Jordaens sample was performed on a Zeiss Axioplan 2 microscope at the Rijksmuseum in Amsterdam. Luminescence images were obtained with a LED 365 nm light source and a filter cube composed of a 365 nm excitation filter (EX G 365), a beamsplitter at 395 nm (BS FT 395) and an emission long-pass filter at 420 nm (EM LP 420). The Zierikzee sample was examined using a Leica DMRX microscope at the FOM Institute AMOLF in Amsterdam. Luminescence images were obtained using an Osram HBO 50 high-pressure mercury lamp and Leica filter cube D, which has an excitation pass filter at 355–425 nm, with a dichroic cutoff filter at 455 nm and a long-pass suppression filter at 470 nm. The van Gogh sample was examined using a Leica DMRX microscope at the National Gallery of Art, Washington. In this case, three filter cubes were used: filter cube D has excitation band-pass filter 355–425 nm with dichroic cut-off filter at 455 nm and long-pass suppression filter 470 nm. Filter cube I3 has excitation band-pass filter 450–490 nm, dichroic filter at 510 nm and a long-pass suppression filter at 515 nm. Filter cube M2 has excitation at band-pass 546/14 dichroic filter at 580 nm and long-pass suppression filter at 590 nm.

SEM backscattered-electron (BSE) images of the Jordaens and Zierikzee samples were obtained on, respectively, an Evo 500 high vacuum electron microscope (Zeiss, Oxford) and on a Verios high-vacuum electron microscope (FEI, Eindhoven, Netherlands) at the FOM Institute AMOLF, Amsterdam.

The ATR-FTIR measurements of the Zierikzee sample were undertaken at the IPANEMA laboratory, Gif-sur-Yvette, France, on a Bruker HYPERION 3000 FTIR microscope using a focal plane array (FPA) detector and an ATR germanium hemisphere crystal.

12.3 Results and Discussion

12.3.1 Lead Soaps

12.3.1.1 Historical Sample (N103 CS9), Jacob Jordaens, *Revolt of the Batavian Against Roman Rule*, 1661–66, Royal Palace Amsterdam

One of the large-scale paintings in the gallery arches of the Citizen's Hall of the Royal Palace Amsterdam depicts *The Revolt of the Batavians against Roman rule* (Fig. 12.1a). The painting has recently undergone conservation and restoration treatment (2005–09). It was glue lined in the eighteenth century, and wax-resin lined in the 1960s. It demonstrates a dramatic darkening, which may have been caused by the combination of aging and past treatments (Froment and Van Eikema Hommes 2011). Extensive lead soap formation in the ground is thought to play a role, and impregnation of the paint with wax and resin from the lining adhesive likely also contributes to color change. The sample studied here was taken from a greenwash to the left side of the moon. The painting was prepared with a double ground. The first beige ground consists of mainly chalk with some (saponified) lead white, a little iron earth pigment with a few umber particles, while the second darker brown ground is composed of lead white, chalk, earth pigment and a relatively higher proportion of umber. On top of the ground layers there is a thin dark gray paint layer with carbon-based black and a little lead white pigment. The second ground is rich in small and large particles and agglomerates of lead white. The sample studied here illustrates a relatively high degree of saponification of the lead white pigment particles in the ground. The opaque lead white particles have converted into lead soaps that have a refractive index similar to the oil binder, causing increased translucency of the paint (Keune et al. 2011; Noble et al. 2008).

The appearance of the second ground layer is striking when observed using UV-A microscopy, which shows highly luminescent particles, as well as particles with a luminescent halo around them (Fig. 12.1c). The SEM backscattered electron image reveals differences in morphology of the lead white pigment particles, which point to lead soap formation. This is supported by the micro-ATR-FTIR imaging data (not shown here). Synchrotron-based photoluminescence (SR-PL) micro-imaging was employed to obtain more detailed information and to investigate the inhomogeneity of the luminescence behavior within the partially saponified lead white paint film.

Figure 12.1 shows the bright-field image, the UV-A-induced luminescence, the SEM backscatter electron image, and SR-PL images obtained upon excitation at 280 nm at two different emission wavelength ranges, 499–529 nm and 641–708 nm. In the SR-PL images collected using $\lambda_{exc} = 280$ nm, contrast is strongly enhanced compared to visualization using UV-A illumination which allows distinguishing the gray surface paint layer (layer II in Fig. 12.1b) and the second ground (layer I in Fig. 12.1b) from each other. It is observed that in the 499–529 nm emission image (Fig. 12.1e) the paint matrix appears much darker (shows less luminescence) in comparison to the 641–708 nm emission image (Fig. 12.1f). Various lead white

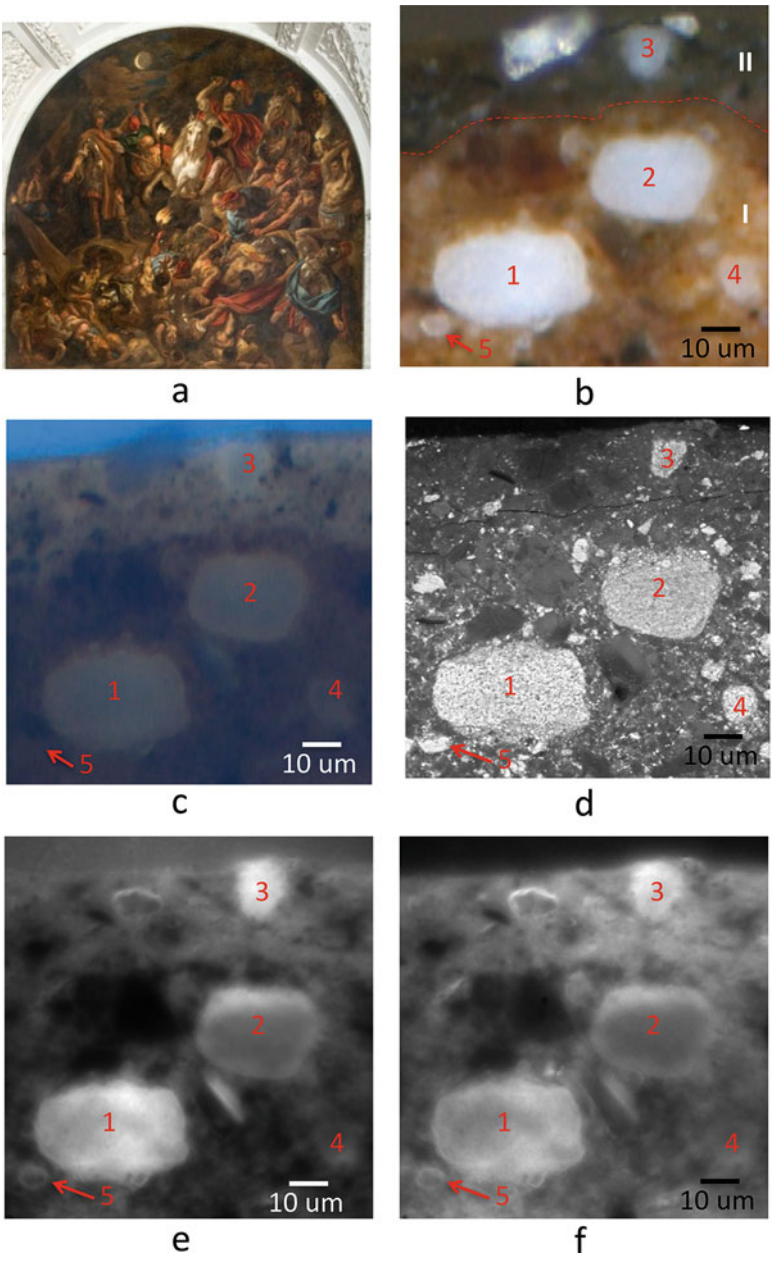

Fig. 12.1 (**a**) *Revolt of the Batavians against Roman rule*, Jacob Jordeans, 1661–66, Royal Palace, Amsterdam, the Netherlands, oil on canvas; (**b**) bright-field image of a sample cross section taken from a green-wash to the left side of the moon showing the gray surface paint layer (II) and the second ground (I); (**c**) UV-A induced microscopic image acquired using a fluorescence microscopy filter cube (filter block ex. 365 nm; em. > 365 nm); (**d**) SEM backscattered-electron image; (**e**) photoluminescence image collected at λ excitation = 280 nm and λ emission = 499–529 nm. Image histogram stretch, 2–98 percentile on the whole image; (**f**) photoluminescence image collected at λ excitation = 280 nm and λ emission = 641–708 nm; image histogram stretch, 2–98 percentile on the whole image

pigment particles/agglomerates (numbered 1–5 in the bright-field image, Fig. 12.1b) show differences in luminescence. Particles 1 and 3 are highly luminescent, while particles 2, 4 and 5 are hardly visible in the SR-PL images. Interestingly, the rim of these particles, however, does exhibit some luminescence. For example, the upper rim of particle 2 luminesces, while the rest of the particle appears dark. Differences in luminescence are visible within the large lead white agglomerate, particle 1. Both the upper and lower rims of this agglomerate exhibit some fluorescence. It is possible to relate the differences in luminescence to the condition/state of the lead white pigment. The SEM backscattered electron image (Fig. 12.1d) shows that the agglomerate of lead white particles (particle 1) has disrupted edges at the upper and lower rims, while the rest of the particle is solid and has clearly defined edges. The same is the case for the upper rim of lead white particle 2, which also looks degraded. Unaltered lead white does not show any detectable luminescence in this emission range (De la Rie 1982). Therefore it can be inferred that the luminescence in the lead white paint is associated with lead soap formation and is a sign of chemical change (MacDonald et al. 2016). The high spatial resolution that was achieved using the SR-photoluminescence imaging allowed visualization of the degradation within one lead white agglomerate. It is known from the literature and from our own experience that pure soaps of long-chain saturated fatty acids do not luminesce on excitation in the deep UV, but the photoluminescence behavior of metal soaps in oil paints may be caused by the presence of disordered states, as suggested by recent studies (Hermans et al. 2015; Martinez-Casado et al. 2014).

12.3.1.2 Historical Sample (ZZ7210_x12), Seventeenth-Century Painted Ceiling in the Room of Trustees, Burgerweeshuis, Zierikzee

In 2014, the seventeenth-century ceiling paintings of allegorical representations in the Room of Trustees, Burgerweeshuis in Zierikzee, underwent an intensive conservation treatment (Fig. 12.2a). The paintings are mounted directly on the wooden planks of the ceiling. In the eighteenth century, they were coated with a thick varnish and had been partly reworked while preserving the seventeenth-century picture beneath. As part of the recent treatment, the later layers of varnish and overpaint were removed revealing the original paint surface that dates to 1680. During the treatment, an earlier red-orange-colored decorative scheme was discovered below the 1680 picture. Various manifestations of lead soap-related degradation phenomena were observed in the multiple paint layers. The focus of this discussion is on the large lead soap aggregates that have formed in the red-orange paint, and how SR-PL was used to visualize multiple phases inside these soap aggregates.

The paint sample discussed here, ZZ7210_x12, was taken from the red sky of the allegorical representation of the reconciliation of Justice (Justitia) and War (Mars), on the west side ceiling located near the fireplace (Fig. 12.2a, right painting). The sample contains the complete layer structure before treatment,

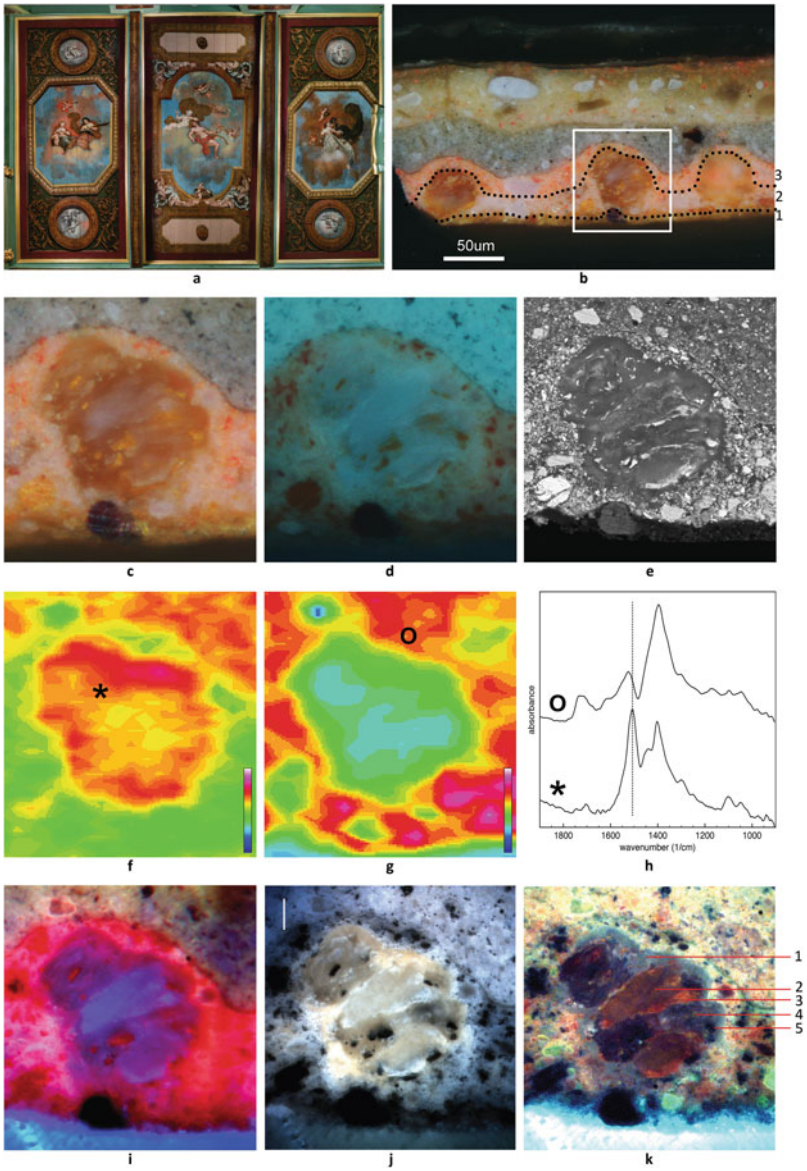

Fig. 12.2 (**a**) Seventeenth-century ceiling painting with allegorical representations, 1680, Room of Trustees, Burgerweeshuis, Zierikzee (Photo: Wim Ruigoord); (**b**) dark-field image of a sample cross section taken from the red sky of *Justitia and Mars in a Warm Embrace*. Photographed at 200×; (**c**) detail of the lead soap aggregate in dark field, corresponding to the white square in (**b**); (**d**) UV-A-induced image of the aggregate using fluorescence microscopy filter cube D (λ excitation = 355–425 nm; λ emission >470 nm); (**e**) SEM backscattered-electron image; (**f**) FTIR image of the *c.*1510 cm^{-1} band in false color (color ranging from blue-low intensity- to purple- high intensity; see inserted color bar) showing the distribution of lead soaps; (**g**) FTIR image of the *c.*1400 cm^{-1} band in false color showing the distribution of lead carbonates;

including the red-orange layers from the earlier decoration, the paint layers from the 1680 allegory, and the eighteenth-century additions (Fig. 12.2b). The red-orange decorative scheme consists of a thin, yellowish ground (layer 1) that contains chalk and earth pigments, followed by a red underlayer (layer 2) with lead white and red lead, and a red surface layer (layer 3) that contains lead white and vermilion. We conclude that the latter was indeed the final layer of a first decorative scheme, because it is covered with a thin surface haze (max. 1 μm thick). This superficial layer has a translucent brown appearance in visible light. EDX reveals it is rich in lead and sulfur. Thin surface layers such as this typically form as a result of interaction between the paint surface and atmospheric compounds (Van Loon 2008; see also the contribution in this Volume by Van Loon et al. on the Pellegrini paintings). Therefore, the red top layer (layer 3) must have been exposed to air for some time before the 1680 painting was commenced.

The lead soap aggregates originate in the red lead-containing layer (layer 2). They have a diameter up to 50 μm and have pushed up the red paint layer that lies on top (layer 3). Both light microscopy and SEM backscattered electron imaging reveal heterogeneity within the lead soap aggregates (Fig. 12.2c–e). Translucent regions visible in the dark-field image (Fig. 12.2c) correspond to the lower scattering (darker) regions in the BSE image (Fig. 12.2e), indicative of a higher organic (low Z) content. Less translucent, whitish regions show a slightly higher scattering (gray) in the BSE image, which points to an increase in lead content, and these regions may contain many dispersed nano-sized particles. In addition, the aggregate contains orange particles of red lead, as well as streaks of opaque whitish particles surrounding the semi-translucent whitish regions. The latter are lead-rich, high scattering (light gray or white) in the BSE. They are very likely re-mineralization products. The ATR-FTIR maps indicate the presence of lead carboxylates (map at *c.*1510 cm^{-1}) inside the aggregate, with a small contribution of carbonates (map at *c.*1400 cm^{-1}), and carbonates more abundantly present in the paint matrix surrounding the aggregate, indicative of unaltered lead white (Fig. 12.2f–g). The maps show some heterogeneity in the distribution of the carboxylate and carbonate bands inside the aggregate. In the FTIR spectrum of the surrounding lead white-containing paint, the position of the asymmetric stretch vibration of the lead carboxylate band ν_{as}(COO-) is shifted from *c.*1510 cm^{-1} to a slightly higher wavenumber (Fig. 12.2h, upper trace). This shift may be caused by lead ions bound

Fig. 12.2 (continued) (**h**) FTIR spectra of 1900–900 cm^{-1} region showing a shift in the position of the lead carboxylate band at *c.*1510 cm^{-1}. Lower trace: spectrum from aggregate. Upper trace: spectrum from surrounding paint matrix; (**i**) false-color photoluminescence emission image; λ excitation = 280 nm; λ emission = 698–766 nm (red), 452–486 nm (green), 370–410 nm (blue). Image histogram stretch, 2–98 percentile on the whole image; (**j**) false-color photoluminescence excitation image acquired using excitation in the UVA; λ emission = 452–486 nm; λ excitation = 380 nm (red), 360 nm (green), 340 nm (blue). Image histogram stretch, 2–98 percentile on the whole image; (**k**) false-color photoluminescence excitation image using excitation in the UVC; λ emission = 452–486 nm; λ excitation = 280 nm (red), 260 nm (green), 240 nm (blue); image histogram stretch, 2–98 percentile on the whole image

to carboxylate groups on the polymerized oil network as in an ionomer (Hermans et al. 2016). The image obtained under UV-A illumination shows luminescence associated with the lead soap aggregate, but it is general and difficult to correlate to the different regions/phases within the aggregate (Fig. 12.2d).

Using the TELEMOS set-up at the DISCO beamline, RGB composite images of the photoluminescence at different emission ranges were obtained. Figure 12.2i shows 698–766 (red channel), 452–486 (green channel) and 370–410 nm (blue channel) for $\lambda_{exc} = 280$ nm. The false color of the aggregate observed in the image varies from red to blue-purple and shows the inhomogeneity of the emission throughout the aggregate. The red lead particles in the aggregate and the surrounding paint layer stand out in the emission image at 698–766 nm (red channel in RGB composite), as well as the vermilion particles present in the red top layer. The purple regions correlate to the translucent regions in the visible light image. The violet regions, which have a high contribution from emission in the 370–410 nm range (blue channel), can be correlated with the more opaque, whitish regions in the visible light image.

Interestingly, visualization of the extent of the inhomogeneity within the aggregate can be improved by using different excitation wavelengths while collecting images of emission over the same ranges. The RGB image collected at 452–486 nm using three different excitation wavelengths in the UV-A $\lambda_{exc} = 380$ (red channel), 360 (green channel) and 340 nm (blue channel) reveals that the aggregate comprises five phases (Fig. 12.2j). The regions at the left and top of the aggregate that appear yellowish could not be distinguished as a separate phase using light microscopy or BSE imaging. The two light gray masses (phase 2) at the center and bottom of the aggregate correspond to the semi-translucent, whitish regions observed in the light microscopy image. Their bright white luminescent rims (phase 3) have excitation-emission behavior similar to the lead-rich particles/streaks in the BSE image. Dark gray-brown regions (phase 4) are visualized in the PL image. These correspond to transparent regions in the light microscopy image. They contain particles of red lead that do not emit and appear black (phase 5).

Comparison of emission images obtained at 452–486 nm upon UV-C excitation $\lambda_{exc} = 280$ (red channel), 260 (green channel) and 240 nm (blue channel) with the UV-A images shows that the metal soap phases have less intense luminescence than on irradiation in the UV-A and, furthermore, the false-color images show more differentiation among phases in the aggregate (Fig. 12.2k). Using UV-C excitation, the core of the aggregate is surrounded by a gray rim (phase 1), which is low scattering (dark) in the BSE image. Brown-reddish masses (phase 2) are noticeable that correspond with the masses that appear light gray under the UV-A excitation image. They show orange-red rims (phase 3), indicating that the luminescence is highest at 280 nm excitation (red channel). Interestingly, the luminescence of the lead white particles in the paint outside the aggregate is the highest at 260 nm excitation (green channel). It can be hypothesized that the re-mineralized products that occur at the orange-red rims (region 3) may be associated with a different lead carbonate phase (possibly neutral lead carbonate) than lead white pigment (mostly basic lead carbonate). Some scattered reddish particles are also visible in the gray

Fig. 12.3 *Roses*, Vincent van Gogh, 1890, National Gallery of Art, Washington. Detail from the background with overall image inset. A high resolution image is available at www.nga.gov

rim, as well as in the dark gray/black masses (phase 4). The red lead particles (phase 5) stand out more in the UV-A excitation image (black particles).

It can be concluded that the luminescence images obtained using different excitation energies have proved that there are a number of lead soap phases inside the aggregate and allow their distribution within the mass to be mapped. Work is under way to understand the origin of the variation in luminescence behavior that could lead to the identification of these phases.

12.3.2 Zinc Soaps

12.3.2.1 Historical Sample, Vincent van Gogh, *Roses*, 1890, Oil on Canvas, National Gallery of Art, Washington

Many paintings have condition problems associated with the use of zinc white paint. Writing to Vincent van Gogh (1853–1890), Paul Gauguin said, "The grape harvests are totally covered in scales as a result of the white which has separated" and he offered a remedy, which he suggested van Gogh might need for his own work (van Gogh Letters 1889). Indeed, the paint films in van Gogh's paintings are sometimes characterized by a chalky, fissured appearance (Osmond et al. 2005). In van Gogh's *Roses* (1890), the paint film in the mint green background is permeated by a network of small fissures that are aligned with the fibers of the canvas (Fig. 12.3). The vertical fissures seem to be more pronounced than the horizontal ones.

A sample from this painting was obtained to examine zinc soap formation using SR-PL imaging. The artist often used a high proportion of zinc white in mixtures, as is the case here. The green paint in the background of *Roses* is made from a mixture of zinc white with emerald green ($Cu(C_2H_3O_2)_2.3Cu(AsO_2)_2$) and a small proportion of a carbon-based black. Only the paint layer is present in the sample. The image obtained in bright field with crossed polars is shown in Fig. 12.4a. The emission of the sample on irradiation using UV-A/VIS excitation on the microscope is shown in Fig. 12.4b. Zinc oxide is a class II–VI semiconductor having a band gap of 2.9–3.45 eV (380–427 nm) and a strong luminescence centered at 384 nm, though particles with crystal defects or impurities have emission at longer wavelengths (Bertrand et al. 2013). In this paint sample, ZnO particles can be seen as small bright dots dispersed throughout the sample due to their strong emission in the visible range. Larger spherical particles of emerald green are dim, and the bulk of the paint, including the fissures, has a generally distributed green or blue-green glow that visually appears relatively homogeneous. Since ZnO absorbs only at wavelengths shorter than ca. 380 nm, the visible-induced emission, shown in Fig. 12.4c, allows observation of luminescence signals produced by species other than ZnO, such as the binding medium. Under these conditions, a diffuse emission from the paint film including in the cracks and fissures is observable; however it is not easy to distinguish by eye between emission from unaltered paint film and zinc soaps.

UV-C excitation and false-color multispectral imaging of the resultant emission clearly differentiate among and offer visualization of the phases that are present, shown by the results illustrated in Fig. 12.4d–f. The images in Fig. 12.4d–f were generated using $\lambda_{exc} = 280$ nm. In (d) emission from particles of ZnO dominate the image since the bad gap emission of ZnO is assigned to the red channel, but areas within the paint film have strong emission bands at 499–520 nm (blue channel) and at 641–708 nm (green channel). Additionally, it can be observed that the fissures are filled with a complex that emits in the UV.

In the zoomed detail of the false-color SR-PL image depicted in (e) the blue channel is used to map emission at 327–353 nm. The phase responsible for this emission completely fills the fissures and cracks in the paint film. It is apparent that this phase and/or another is present in “hot spots” that are magenta/purple in the image evident, for example, at the center of the field of view in the false-color image (e). A similar emission profile is present around individual particles of emerald green suggesting a chemical similarity between the hot spots and the periphery of the particles of emerald green. The highest zoom of the false-color SR-PL image (f) shows that the luminescence of zinc oxide particles (appearing red) seem to be unaltered. Therefore, zinc soap formation is not ongoing at these boundaries. These results suggest that soap formation does not begin at cracks and fissures, but once formed, soaps aggregate within fissures and likely cause their expansion.

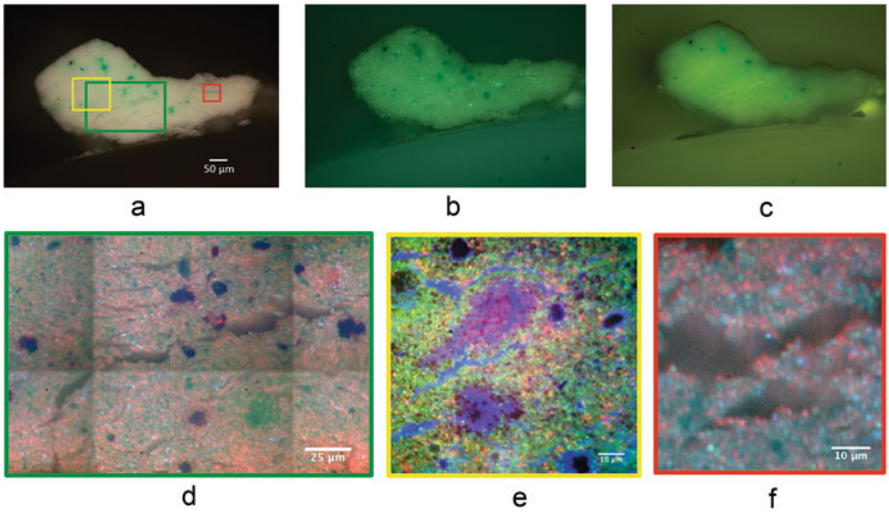

Fig. 12.4 Images of a sample cross section taken from the background of *Roses*, by Vincent van Gogh. (**a**) Bright-field (crossed polars) image showing that the paint is made from a mixture of zinc white, emerald green, and a carbon black; (**b**) the sample viewed using fluorescence microscopy filter cubes D (excitation band-pass 355–425 nm, dichroic filter 455 nm, and long-pass filter 470 nm); (**c**) fluorescence microscopy filter I3 (excitation band-pass filter 450–490 nm, dichroic filter 510 nm, and long-pass filter 515 nm); (**d**) detail corresponding to the green rectangle in **a** at 100×. λ excitation = 280 nm. λ emission of false-color image channels = 370–410 nm (red); G: 641–708 nm (green); B: 499–529 nm (blue). Image histogram stretch: square root on the whole image; (**e**) zoom of false-color PL image corresponding to the yellow rectangle in (**a**) at 100×. λ excitation = 280 nm. λ emission of false-color image channels = 452–486 nm (red); 370–410 nm (green); 327–353 nm (blue). Image histogram stretch: equalization on the zoomed area; (**f**) zoom of the false-color PL image corresponding the red rectangle in (a) at 100×. λ excitation = 280 nm. λ emission of false-color image channels = 370–410 nm (red); 698–766 nm (green); 641–708 nm (blue)

12.4 Conclusions

Synchrotron deep-UV photoluminescence micro-imaging has provided unprecedented information to help analyze the chemical complexity of metal soap formation and their aggregation. Taking advantage of the high spatial resolution of synchrotron PL imaging, we characterized early stages of reaction in a paint film occurring at the edges of individual lead white particles as well as at the interface of flocs of particles with the binder. The emission spectra of phases formed during the initial processes and later the development of aggregates of soaps have been shown to be different. The results indicate that there are many chemical phases present during the process of soap aggregate formation, and also within the final large lead soap protrusions. Here a larger number of phases than expected from traditional fluorescence microscopy or SEM-EDX was discovered. This finding was possible because the technique provides emission contrast at the sub-micron scale, allowing

individual particles to be observed. The information obtained is distinct from and complementary to speciation using other techniques such as FTIR and SEM and elemental analyses.

Chemical alteration can be identified and located at an early stage of development and relatively low degree of degradation. In the case of zinc soap formation, it was observed that areas of alteration develop within the paint film and, in the case studied here, occurs around particles of emerald green. The alteration products do not appear to be developing at fissures, and soap formation is not active at their edges or at micro-cracks; however, soaps appear to aggregate within these cracks and this may be the cause of their expansion.

Ongoing work is aiming to use synchrotron PL to study the phenomena associated with soap formation in a much larger corpus of micro-samples to obtain information on the number of chemical species involved in the various processes of soap formation and robust chemical identification using PL characteristics and other techniques.

Acknowledgments This work is part of the PAinT project, supported by the Science4Arts program of the Dutch Organization for Scientific Research (NWO). We wish to thank Emilie Froment (University of Amsterdam) for providing the paint sample of Jacob Jordaens' *Revolt of the Batavian against Roman Rule*, Royal Palace, Amsterdam. We are also indebted to Roos Keppler and Annefloor Schlotter (independent conservators of historic interiors, the Netherlands) for providing the paint sample of the seventeenth-century painted ceiling in the Room of Trustees, Burgerweeshuis, Zierikzee.

References

Bertrand L, Réfrégiers M, Berrie B, Échard J-P, Thoury M (2013) A multiscalar photoluminescence approach to discriminate among semiconducting historical zinc white pigments. Analyst 138:4463–4469. https://doi.org/10.1039/c3an36874b

De la Rie RE (1982) Fluorescence of paint and varnish layers (part II). Stud Conserv 27(2):65–69

Froment E, Van Eikema Hommes MH (2011) The darkness of the nocturnal conspiracy of Claudius Civilis by Govert Flinck and Jürgen Ovens (1659–1662) in the Royal Palace Amsterdam. In: Bridgland J (ed) Preprints ICOM committee for conservation, 16th triennial meeting, Lisbon, 19–23 Sept

Giuliani A, Jamme F, Rouam V, Wien F, Giorgetta J-L, Lagarde B, Chubar O, Bac S, Yao I, Rey S, Herbeux C, Marlats JL, Zerbib D, Polack F, Réfrégiers M (2009) DISCO: a low-energy multipurpose beamline at synchrotron SOLEIL. J Synchrotron Radiat 16:835–841

Hermans JJ, Keune K, Van Loon A, Iedema PD (2015) An infrared spectroscopic study of the nature of zinc carboxylates in oil paintings. J Anal At Spectrom 30:1600–1608. https://doi.org/10.1039/c5ja00120j

Hermans JJ, Keune K, Van Loon A, Corkery RW, Iedema P (2016) Ionomer-like structure in mature oil paint binding media. RSC Adv 6:93363–93369. https://doi.org/10.1039/C6RA18267D

Higgitt C, Spring M, Saunders D (2003) Pigment-medium interactions in oil paint films containing red lead or lead-tin yellow. Natl Gallery Tech Bull 24:75–95

Keune K, Van Loon A, Boon J (2011) SEM backscattered-electron images of paint cross-sections as information source for the presence of the lead white pigment and lead-related degradation and migration phenomena in oil paintings. Microsc Microanal 17(5):696–701. https://doi.org/10.1017/S1431927610094444

MacDonald MG, Palmer MR, Suchomel MR, Berrie BH (2016) Reaction of Pb(II) and Zn(II) with ethyl linoleate to form structured hybrid inorganic–organic complexes: a model for degradation in historic paint films. ACS Omega 1(3):44–50. https://doi.org/10.1021/acsomega.6b00075

Martinez-Casado FJ et al (2014) Short lead(II) soaps: from weakly fluorescent crystals to strongly phosphorescent and structurally varied vitreous phases. A thermal, structural and spectroscopic study. J Mater Chem C 2:9489–9496. https://doi.org/10.1039/c4tc01645a

Noble P, Boon JJ, Wadum J (2002) Dissolution, aggregation and protrusion: lead soap formation in 17th century grounds and paint layers. In: Art matters, Netherlands technical studies in art, Waanders Publishers, Zwolle, pp 46–61

Noble P, Van Loon A, Boon JJ (2008) Selective darkening of ground layers associated with the wood grain in 17th-century panel paintings. In: Townsend J, Doherty T, Heydenreich G, Ridge J (eds) Postprints ICOM committee for conservation interim meeting, London, June 2007, pp 68–78

Osmond G, Keune K, Boon J (2005) A study of zinc soap aggregated in a late 19th century painting by R.G. Rivers at the Queensland art gallery. AIC CM Bull 29:37–46

Thoury M, Echard J-P, Réfrégiers M, Berrie B, Nevin A, Jamme F, Bertrand L (2011) Synchrotron UV-visible multispectral luminescence micro-imaging of historical samples. Anal Chem 83(5):1737–1745

Van Gogh Letters (734 Br. 1990: 739|CL: GAC 34 Date: Paris, between Tuesday, 8 and Wednesday, 16 January 1889). Les vendanges sont en totalité écaillées par suite du blanc qui s'est separé. http://vangoghletters.org/vg/letters/let734/letter.html

Van Loon A (2008) White hazes and surface crusts on dark oil paint films. In: Color changes and chemical reactivity in seventeenth-century oil paints. PhD dissertation, University of Amsterdam, Molart series (14), AMOLF, Amsterdam. Downloadable from http://www.amolf.nl/publications

Van Loon A, Keune K, Boon JJ (2005) Improving the surface quality of paint cross-sections for imaging analytical studies with specular reflection FTIR and static-SIMS. In: Proceedings of art'05 conference on non-destructive testing and microanalysis for the diagnostics and conservation of the cultural and environmental heritage, Lecce, Italy, May 15–19, 2005 (CD-ROM)